

UC Irvine

UC Irvine Previously Published Works

Title

Using localized double-quantum-coherence spectroscopy to reconstruct the two-exciton wave function of coupled quantum emitters

Permalink

<https://escholarship.org/uc/item/5vk5q4vt>

Journal

New Journal of Physics, 15(2)

ISSN

1367-2630

Authors

Schlosser, Felix
Knorr, Andreas
Mukamel, Shaul
[et al.](#)

Publication Date

2013-02-05

DOI

10.1088/1367-2630/15/2/025004

Copyright Information

This work is made available under the terms of a Creative Commons Attribution License, available at <https://creativecommons.org/licenses/by/4.0/>

Peer reviewed

Using localized double-quantum-coherence spectroscopy to reconstruct the two-exciton wave function of coupled quantum emitters

Felix Schlosser¹, Andreas Knorr¹, Shaul Mukamel²
and Marten Richter^{1,3}

¹ Institut für Theoretische Physik, Nichtlineare Optik und Quantenelektronik, Technische Universität Berlin, Hardenbergstraße 36, 10623 Berlin, Germany

² Department of Chemistry, University of California, Irvine, CA 92697-2025, USA

E-mail: marten.richter@tu-berlin.de

New Journal of Physics **15** (2013) 025004 (23pp)

Received 18 September 2012

Published 5 February 2013

Online at <http://www.njp.org/>

doi:10.1088/1367-2630/15/2/025004

Abstract. Coherent multidimensional spectroscopy allows us to inspect the energies and the coupling of quantum systems. Coupled quantum systems—such as a coupled semiconductor quantum dot or pigments in photosynthesis—form delocalized exciton and two-exciton states. A technique is presented to decompose these delocalized wave functions into the basis of individual quantum emitters. This quantum state tomography protocol is illustrated for three coupled InAs quantum dots. To achieve the decomposition of the wavefunction, we combine the double-quantum-coherence spectroscopy with spatiotemporal control, which allows us to localize optical excitations at a specific quantum dot. Recently, a protocol was proposed for single exciton states (Richter *et al* 2012 *Phys. Rev. B* **86** 085308). In this paper, we extend the method presented by Richter *et al* with respect to: the reconstruction of two-exciton states, a detailed analysis process of reconstruction and the effect of filtering to enhance the quality of the reconstructed wave function.

³ Author to whom any correspondence should be addressed.



Content from this work may be used under the terms of the [Creative Commons Attribution-NonCommercial-ShareAlike 3.0 licence](https://creativecommons.org/licenses/by-nc-sa/3.0/). Any further distribution of this work must maintain attribution to the author(s) and the title of the work, journal citation and DOI.

Contents

1. Introduction	2
2. Two-dimensional (2D) spectroscopy	3
2.1. Setup and simulation	3
2.2. Coupled quantum dots	4
2.3. 2D spectra	6
3. Localized spectroscopy	8
3.1. Spatiotemporal control	8
3.2. Localized spectra	8
3.3. Localization of the first pulse	9
3.4. Localization of the first and second pulses	10
3.5. Localization of the second pulse	11
3.6. Reconstruction of the wave functions	13
3.7. Filtering different resonances	18
4. Applicability of the reconstruction	20
5. Conclusion	21
Acknowledgments	21
References	21

1. Introduction

Complex (hybrid) nanostructures are often formed by combining different individual nanostructures such as metal nanoparticles, semiconductor quantum dots (QDs), pigments embedded in proteins, such as in light harvesting complexes and J-aggregates [1–10]. Couplings (such as Coulomb couplings) between the individual emitters lead to the formation of new quantum states delocalized over the individual nanostructure.

Far-field optical experiments cannot resolve the internal structure of the delocalized states since the applied electric field is spatially constant on the spatial dimension of the nanostructure, which is much smaller than the excitation wavelength. Therefore only the collective formed delocalized exciton states are accessible in far-field spectroscopy. For disentangling the individual contributions to delocalized states, a form of near-field spectroscopy is needed. There have recently been many experiments demonstrating that spatiotemporal control of optical excitations can be achieved by combining pulse shaping techniques with nanoplasmonics [11–13]. There are also even experiments that demonstrate how nanometer spatial resolution and two-dimensional (2D) spectroscopy can be combined [14]. Other techniques for spatiotemporal control include near-field techniques such as (metalized) fiber tips [1, 12, 15–17] or nano-antennas [18–23].

While nonlinear 1D spectroscopy provides the energy and spectral shape of exciting coupled quantum systems, coherent multidimensional spectroscopy allows to also investigate the couplings between the states [24, 25]. Multidimensional spectroscopy gives a deeper insight into the underlying microscopic processes.

Combining coherent multidimensional spectroscopy with spatiotemporal control of exciting pulses promises to reveal more information about the system than 2D spectroscopy

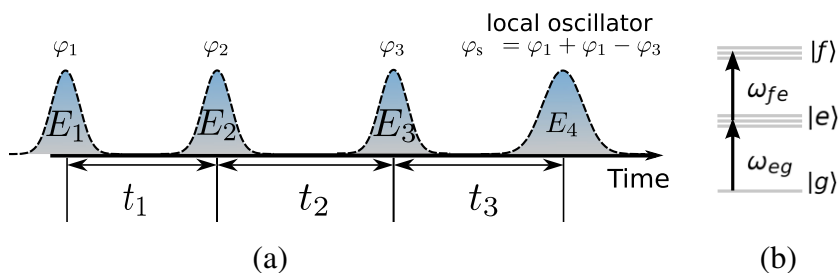


Figure 1. In (a), the pulse sequence of the double-quantum-coherence signal is shown. Part (b) illustrates the delocalized states of the coupled QD system.

or localization alone [14]. We extend the reconstruction method for delocalized single excitons presented in [26] from single excitons to two excitons.

In section 2, double-quantum coherence 2D spectroscopy is described [24]. After presenting the double-quantum coherent spectroscopy [24, 27, 28], the treatment of the coupling of the QDs is described. Then, 2D spectra and their signal are discussed. In section 3, the focus is on localized spectroscopy: firstly, examples of spatiotemporal control are explained; next, the description of the spectra from section 2 is generalized to localized excitation. Then, the method of reconstructing the exciton as well as the two-exciton wave function coefficients is presented in detail. Finally, the filtering method—introduced in more detail in [26]—is applied to improve the quality of reconstruction. Here, we discuss also quantitatively the influence of filtering on the reconstruction. The paper is aimed at an extension of the methods from [26] towards determination of two-exciton wave functions.

2. Two-dimensional (2D) spectroscopy

1D nonlinear spectroscopy techniques such as pump–probe or four-wave mixing experiments allow us to investigate the time evolution of quantum states and transition energy of the excited states.

Coherent multidimensional spectroscopy [12, 24, 27–37] provides new insights into the structure of several complex molecular and nanoscale systems such as photosynthetic aggregates or semiconductors [1, 2, 7, 24, 38]. Recently, even the application of coherent spectroscopy to GaAs natural QDs was reported [39–41]. Coherent spectroscopy uses multiple excitation pulses together with direction selection or phase cycling to control the quantum pathways of excitation. The delay times between the pulses are varied giving a signal dependent on multiple dimensions.

2.1. Setup and simulation

In four-wave mixing experiments the sample is excited by a sequence of three pulse envelopes

$$E(r, t) = E^1(r, t - t_3 - t_2 - t_1)e^{i\omega_1(t-t_3-t_2-t_1)+i\varphi_1} + E^2(r, t - t_3 - t_2)e^{i\omega_1(t-t_3-t_2)+i\varphi_2} \\ + E^3(r, t - t_3)e^{i\omega_1(t-t_3)+i\varphi_3} + \text{c.c.}$$

separated by variable time delays t_1, t_2 and t_3 with different phases φ_1, φ_2 and φ_3 and laser frequency ω_1 (illustrated in figure 1(a)). Since we treat only a single nanostructure, a dissection

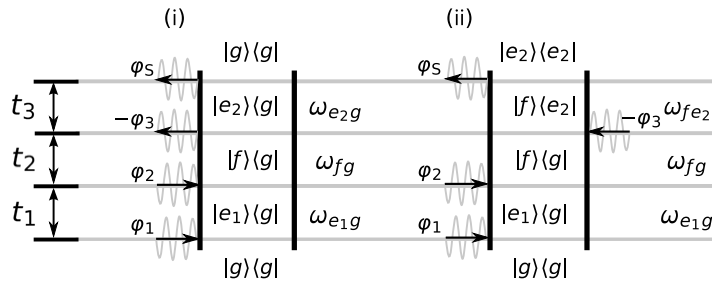


Figure 2. Double-sided Feynman diagram that shows two possible pathways for the DQCS.

of quantum pathways using the direction of the incoming fields is not possible. Therefore, a phase cycling technique is applied. Here, the simulated experiment is carried out several times with different phase contributions φ_1 , φ_2 and φ_3 . This allows us to extract a specific signal, described by the linear combination $\varphi_s = l\varphi_1 + m\varphi_2 + n\varphi_3$ of the phases using postprocessing algorithms (where l , n and m are integers). To extract a certain polarization $P_{l,m,n}$ from the detected polarization $P(t, \varphi_1, \varphi_2, \varphi_3) = \sum_{l,m,n} P_{l,m,n}(t)e^{i(l\varphi_1+m\varphi_2+n\varphi_3)}$, the experiment is repeated for sufficient phase combinations [42] (determined by the matrix $e^{i(l\varphi_1+m\varphi_2+n\varphi_3)}$), so that the polarization $P_{l,m,n}$ can be extracted by inverting the matrix $e^{i(l\varphi_1+m\varphi_2+n\varphi_3)}$.

In this paper, we focus on double-quantum-coherence spectroscopy (DQCS), where the extracted phase combination is $\varphi_{\text{III}} = \varphi_1 + \varphi_2 - \varphi_3$. Two Liouville pathways contribute to this signal for a three-band system as depicted in figure 1(b). The pathways are shown in figure 2, presented by double-sided Feynman diagrams [29]: in both quantum pathways, the first pulse creates a coherence between the ground state and a single exciton, and the second pulse creates a coherence between a two-exciton and the ground state. The third pulse creates in pathway (i) a single exciton to ground state coherence, whereas in pathway (ii) a two-exciton to single exciton coherence is created. The fourth pulse depicted in figure 1(a) is the local oscillator for heterodyne detection [24]. This allows a detection of the signal phase.

2.2. Coupled quantum dots

In the following, QDs—as an example of a system of coupled nanostructures—are examined in the 2D spectroscopy experiment. We will demonstrate that the DQCS can reveal the energy of single and two-exciton states of the coupled QDs [24, 43].

As a model system, we examine $n = 3$ coupled QDs that are spatially close enough to couple via Förster coupling but spatially separated enough to have no wave function overlap. Such a coupling is even possible by assuming that the wave functions do not overlap.

The local single exciton basis elements of n two-level QDs are the n basis elements $|i\rangle$, where $|i\rangle$ means that only QD i is excited and the other QDs are in the ground state. The $n(n-1)/2$ two-exciton basis elements are $|ij\rangle$, where $|ij\rangle$ means that only QD i and j are in excited states and all other QDs are in ground states. We restrict the discussion to a maximum of two excitations, which is sufficient for spectroscopy in third order of the optical field. The ground state of the whole nanostructure is denoted by $|g\rangle$. The Hamiltonian $H = H_0 + H_C + H_{e-1}$ consists of three parts: H_0 , which corresponds to the energy of the electron in the isolated

uncoupled system, the field–matter interaction H_{e-1} , which describes the dipole coupling to a classical electric field, and the Coulomb interaction H_C . They are given by

$$H_0 = \epsilon_0 |g\rangle\langle g| + \sum_i^n \epsilon_i |i\rangle\langle i| + \sum_{i<j} (\epsilon_i + \epsilon_j) |ij\rangle\langle ij|, \quad (1a)$$

$$H_C = \sum_{i<j} V_{ij} |ij\rangle\langle ij| + \sum_{i,j\neq i} V_{ij}^F |i\rangle\langle j| + \sum_{k,i\neq k,j\neq k} V_{ij}^F |ki\rangle\langle kj|, \quad (1b)$$

$$H_{e-1} = \sum_i^n \mu_{gi} \cdot E(t) |g\rangle\langle i| + \sum_{i,j\neq i} \mu_{ij} \cdot E(t) |i\rangle\langle ij| + \text{h.a.} \quad (1c)$$

with the energies ϵ and the coupling parameters⁴. The chosen parameters for the size and the distances of the QDs for our example system and their energy shifts and coupling constants are adjusted to be in the order of known theoretical [44] and experimental data [45]. Note that the form of our Hamiltonian is quite general. Other types of QDs, nanocrystals or chlorophyll molecules can be described by the same form of Hamiltonian. Therefore, the presented method can be applied to a broad range of materials.

Coulomb coupling H_C between the QDs leads to the formation of delocalized states. These delocalized single exciton $|e\rangle$ and two-exciton states $|f\rangle$ can be written as a linear combination of the local basis

$$|e\rangle = \sum_i^n c_i^e |i\rangle, \quad |f\rangle = \sum_{i,j\neq i}^n c_{ij}^f |ij\rangle, \quad (2)$$

for single exciton states and two-exciton states, respectively. These states are obtained by diagonalizing the Hamiltonian $H_0 + H_C$ including the coupling between the nanostructures (see figure 1(b)).

The pure electronic part of the Hamiltonian reads in delocalized basis

$$H_0 + H_C = \hbar\omega_g |g\rangle\langle g| + \sum_e \hbar\omega_e |e\rangle\langle e| + \sum_f \hbar\omega_f |f\rangle\langle f|$$

with ϵ_g , ϵ_e and ϵ_f as the eigenenergy for the ground state, the single-exciton state and the double-exciton state, respectively. For rewriting the field–matter part of equation (1c) in a delocalized basis, we use the inverse transformation for single excitons $|i\rangle = \sum_e c_i^{e*} |e\rangle$ and two-exciton states $|ij\rangle = \sum_f c_{ij}^{f*} |f\rangle$. With these relations, the electron light coupling Hamiltonian in delocalized basis reads

$$\begin{aligned} H_{e-1} &= \sum_i^n \sum_e c_i^e \mu_{gi} \cdot E(t) |g\rangle\langle e| + \sum_{i,j\neq i}^n \sum_{e,f} c_i^{e*} c_{ij}^f \mu_{gj} \cdot E(t) |e\rangle\langle f| + \text{h. a.} \\ &= \sum_e \mu_{ge} \cdot E(t) |g\rangle\langle e| + \sum_{e,f} \mu_{ef} \cdot E(t) |e\rangle\langle f| + \text{h. a.} \end{aligned} \quad (3)$$

⁴ For the following calculations we choose as parameters for the model system: $\epsilon_0 = 0 \mu\text{eV}$, $\epsilon_1 = -2.2 \mu\text{eV}$, $\epsilon_2 = 0.2 \mu\text{eV}$, $\epsilon_3 = 2.5 \mu\text{eV}$, $V_{12}^F = -0.4 \mu\text{eV}$, $V_{13}^F = -0.6 \mu\text{eV}$, $V_{23}^F = -0.3 \mu\text{eV}$, $V_{12} = -0.4 \mu\text{eV}$, $V_{13} = 0.2 \mu\text{eV}$ and $V_{23} = 0.8 \mu\text{eV}$.

with the dipole moments in delocalized basis

$$\mu_{ge} = \sum_i^n c_i^e \mu_{gi} \quad \text{and} \quad \mu_{ef} = \sum_{i,j \neq i}^n c_i^{e*} \mu_{gj} c_{ij}^f \quad (4)$$

for ground state to single exciton and single exciton to two-exciton transitions, respectively.

2.3. 2D spectra

The signal of 2D spectroscopy is measured in dependence of the three delay times t_1 , t_2 and t_3 between the pulses (cf figure 1(a)). The spectroscopic signal is measured using heterodyne detection, where the polarization induced by the three pulses is mixed with a local oscillator [24]:

$$S_{\varphi_{\text{III}}}^{(3)}(t_1, t_2, t_3) = \int_{-\infty}^{\infty} dt P_{\varphi_{\text{III}}}^{(3)}(t) E^{4*}(t) e^{i\omega t} \quad (5)$$

to be able to extract the real and imaginary parts of the signal. Phase cycling ensures that we only retrieve the contributions from the polarization with phase combination $\phi_{\text{III}} = \phi_1 + \phi_2 - \phi_3$. The polarization connected to ϕ_{III} generated by the three pulses can be described using response functions [24]:

$$P_{\varphi_{\text{III}}}^{(3)}(t) = \int_0^{\infty} d\tau_3 \int_0^{\infty} d\tau_2 \int_0^{\infty} d\tau_1 R_{\varphi_{\text{III}}}^{(3)}(t, t - \tau_3, t - \tau_3 - \tau_2, t - \tau_3 - \tau_2 - \tau_1). \quad (6)$$

For the case of our three-band model, only the processes depicted in the two Liouville diagrams in figure 2 contribute, leading to

$$R_{\varphi_{\text{III}}}^{(3)}(t, \tilde{t}_3, \tilde{t}_2, \tilde{t}_1) = R_i^{(3)}(t, \tilde{t}_3, \tilde{t}_2, \tilde{t}_1) + R_{ii}^{(3)}(t, \tilde{t}_3, \tilde{t}_2, \tilde{t}_1) \quad (7)$$

$$\begin{aligned} R_i^{(3)}(t, \tilde{t}_3, \tilde{t}_2, \tilde{t}_1) = & - \left(\frac{i}{\hbar} \right)^3 e^{i\omega(\tilde{t}_1 + \tilde{t}_2 - \tilde{t}_3 - t_1 - 2t_2 - t_3)} \\ & \sum_{ee'f} \mu_{e'f} \mu_{ge'} \cdot E^{3*}(\tilde{t}_3 - t_3) \mu_{fe} \cdot E^2(\tilde{t}_2 - t_3 - t_2) \mu_{eg} \cdot E^1(\tilde{t}_1 - t_3 - t_2 - t_1) \\ & e^{-i\xi_{fe'}(t - \tilde{t}_3) - i\xi_{fg}(\tilde{t}_3 - \tilde{t}_2) - i\xi_{eg}(\tilde{t}_2 - \tilde{t}_1)} \end{aligned} \quad (8)$$

$$\begin{aligned} R_{ii}^{(3)}(t, \tilde{t}_3, \tilde{t}_2, \tilde{t}_1) = & \left(\frac{i}{\hbar} \right)^3 e^{i\omega(\tilde{t}_1 + \tilde{t}_2 - \tilde{t}_3 - t_1 - 2t_2 - t_3)} \\ & \sum_{ee'f} \mu_{ge'} \mu_{e'f} \cdot E^{3*}(\tilde{t}_3 - t_3) \mu_{fe} \cdot E^2(\tilde{t}_2 - t_3 - t_2) \mu_{eg} \cdot E^1(\tilde{t}_1 - t_3 - t_2 - t_1) \\ & e^{-i\xi_{e'g}(t - \tilde{t}_3) - i\xi_{fg}(\tilde{t}_3 - \tilde{t}_2) - i\xi_{eg}(\tilde{t}_2 - \tilde{t}_1)}. \end{aligned} \quad (9)$$

Here, we introduced the frequencies $\omega_{ij} = \omega_i - \omega_j$, with the exciton energies $\hbar\omega_i$, and $\xi_{ij} = \omega_{ij} + i\gamma_{ij}$ with the dephasing γ_{ij} . The first pulse induces in both pathways a coherence between the ground state and a single exciton state. The second pulses then create a quantum coherence between the ground state and a two-exciton state from the ground state to single exciton coherence, giving the method its name double-quantum coherence. After the third pulses both

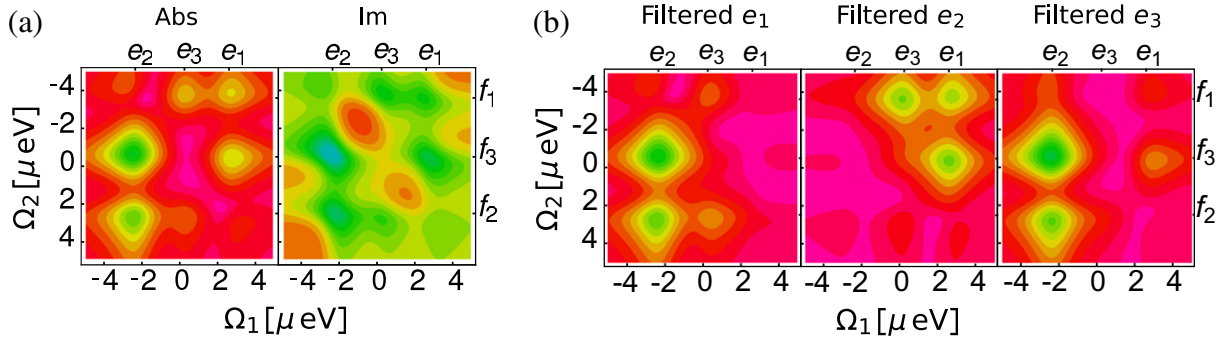


Figure 3. Double-quantum-coherence signal with $t_3 = 20$ ps. In (a), the absolute value is shown on the left; the imaginary part of the full spectrum is shown on the right. Part (b) illustrates the filtered spectrum for each resonance. The detection frequencies are given as detuning around the single and the double gap frequency, respectively.

pathways differ having either a ground state to single exciton coherence or a single exciton to two-exciton coherence.

A Fourier transform of the signal $S_{\varphi_{\text{III}}}(t_1, t_2, t_3)$ with respect to two of the three time intervals at a fixed third time interval retrieves the 2D spectrum:

$$S_{\varphi_{\text{III}}}^{(3)}(\Omega_1, \Omega_2, t_3) = \int_0^\infty dt_1 \int_0^\infty dt_2 e^{i\Omega_1 t_1 + i\Omega_2 t_2} S_{k_{\text{III}}}^{(3)}(t_1, t_2, t_3). \quad (10)$$

For the DQCS, we take the Fourier transform with respect to the time intervals t_1 and t_2 , so that the signal depends on the single and two-exciton frequencies Ω_1 and Ω_2 , respectively. The far-field double-quantum-coherence signal reads

$$S_{\varphi_{\text{III}}}^{(3)}(\Omega_1, \Omega_2, t_3) = S_{\text{i}}^{(3)}(\Omega_1, \Omega_2, t_3) + S_{\text{ii}}^{(3)}(\Omega_1, \Omega_2, t_3) \quad (11)$$

with

$$S_{\text{i}}^{(3)}(\Omega_1, \Omega_2, t_3) = \frac{1}{\hbar^3} \sum_{e, e', f} \mu_{e'f} \cdot E_4^*(\omega_{fe'}) \mu_{ge'} \cdot E_3^*(\omega_{e'g}) \mu_{ef}^* \cdot E_2(\omega_{fe}) \\ \times \mu_{ge}^* \cdot E_1(\omega_{eg}) \frac{e^{-i\xi_{fe'} t_3}}{(\Omega_2 - \xi_{fg})(\Omega_1 - \xi_{eg})}$$

and

$$S_{\text{ii}}^{(3)}(\Omega_1, \Omega_2, t_3) = -\frac{1}{\hbar^3} \sum_{e, e', f} \mu_{ge'} \cdot E_4^*(\omega_{e'g}) \mu_{ef} \cdot E_3^*(\omega_{fe'}) \\ \times \mu_{ef}^* \cdot E_2(\omega_{fe}) \mu_{ge}^* \cdot E_1(\omega_{eg}) \frac{e^{-i\xi_{e'g} t_3}}{(\Omega_2 - \xi_{fg})(\Omega_1 - \xi_{eg})},$$

with $E_k(\omega)$ as the Fourier transformation of the electric field envelopes for the pulses $k = 1, 2, 3, 4$. The signal consists of the contributions of two Liouville pathways for the case of the three-band system formed from ground state, single excitons and two excitons.

An example is given on the left in figure 3(a) for the absolute value of the spectrum. Here, the detection frequencies are given as detuning around the single and the double gap

frequency, respectively. The right plot in figure 3(a) shows the corresponding imaginary part. We assumed that the spectral bandwidth of the exciting pulses is much larger than the bandwidth of the exciton energy and therefore we assume a constant $E_i(\omega) = E_i$.

In these 2D spectra, we see several resonances that connect the single-exciton state at energy $\omega_{e_i,g}$ to the two-exciton states at $\omega_{f_i,g}$. The strength is a qualitative indicator of which delocalized single states contribute to which two-exciton state. For example, from figure 3(a), we see that f_1 is mainly connected to e_3 and e_1 , whereas f_2 is mainly connected to e_2 and e_3 , and f_3 to e_1 and e_2 . Note that the strength of the resonances is only a hint of the connection between these states due to interference effects.

Note that in most experimental realizations, a Fourier transform of the second and third delay times is recorded. Since the Fourier transformation of the last third delay time can be recorded using a spectrometer, this makes the experiment more feasible. The latter presented method for extracting the two-exciton coefficients will also work in this configuration, since the algorithm relies on the second delay time. The method for extracting the single exciton wave function needs to be used together with a photon echo φ_I with a 2D spectra of the first and third delay times, since it relies on a localization of the pulse at the first delay time.

3. Localized spectroscopy

We will now combine the DQCS technique with localized fields to reveal more information than in a far-field DQCS. The first section summarizes modern experiments that achieve localized excitations with a nanometer resolution well below the diffraction limit. In the second part, we will show 2D spectra calculated with localized pulses and point out the additional information retrievable with localization. In the last part, algorithms which use localized 2D spectroscopy are presented, e.g. for reconstructing the delocalized wave function. Protocols applicable for single exciton states and two-exciton states will be presented.

3.1. Spatiotemporal control

The objective for our localized spectroscopy is controlling optical excitations in such a way that just one emitter in a coupled nanostructure becomes locally excited. Realizing field localization on a nanometer length scale can be fulfilled using different methods. The presented protocols in this work do not depend on the particular method. It is only important that one emitter of the coupled quantum system can be excited about a factor of 10 higher than the others in terms of the electric field in order to achieve a good reconstruction of the delocalized exciton states.

In addition to near-field spectroscopy with coated [1] and uncoated fiber tips [15] or metal tips [12, 16, 17], there exist also metal nano-antennas [18–23] for controlling fields on the nanoscale.

3.2. Localized spectra

In this section, we apply a localization technique as motivated in section 3.1. We replace one or two pulses of the pulse sequence with pulses localized, so that it excites only a single QD. All other pulses still excite all dots equally. We will start with a modified description of the signal. Then we present calculated spectra.

In order to describe this in our framework, we have to adapt the Hamiltonian for localized excitation. In the local basis, it is obvious that we have to take the electric field at the position of the QD:

$$H_{\text{el-L}} = \sum_i \mu_{gi} \cdot E(r_i, t) |g\rangle \langle i| + \sum_{ij} \mu_{gi} \cdot E(r_i, t) |j\rangle \langle ij| + \text{h.a.} \quad (12)$$

In order to express $H_{\text{el-L}}$ in the delocalized states, we can insert the expansion of the local states in terms of the delocalized exciton states:

$$H_{\text{el-L}} = \sum_{ie} c_i^e \mu_{gi} \cdot E(r_i, t) |g\rangle \langle e| + \sum_{i < jef} c_i^{e*} \mu_{gi} c_{ij}^f \cdot E(r_i, t) |e\rangle \langle f| + \text{h.a.} \quad (13)$$

We note that we cannot formulate the dipole moments in terms of delocalized dipole moments for near-field distributions. This can only be done in far-field excitation assuming constant electric fields over the whole nanostructure. Note that the far-field Hamilton-operator equation (3) can be obtained from the localized form by assuming a spatial constant electric field over the whole nanostructure.

3.3. Localization of the first pulse

For the first modification of the DQCS signal, we use a localization of the first pulse of the sequence. This will control the QDs involved in the ground state to single exciton transition. For this purpose, equation (11) can be rewritten using the Hamiltonian reformulated in localized fields for the first interaction. Assuming a perfect local excitation, the spatial field distribution of the localized first pulse can be written as $E_{1,i}^{\text{loc}}(r_k) = E_{1,i}^{\text{loc}} \delta_{ik}$ if QD i is the excited dot. Thus, the sum over the QD number k vanishes and the simplified signal reads

$$S_{E_1}^{\text{loc}}(i, \Omega_1, \Omega_2, t_3) = S_{E_{1,i}}^{\text{loc}}(i, \Omega_1, \Omega_2, t_3) + S_{E_{1,ii}}^{\text{loc}}(i, \Omega_1, \Omega_2, t_3) \quad (14)$$

with

$$S_{E_{1,i}}^{\text{loc}}(i, \Omega_1, \Omega_2, t_3) = \frac{1}{\hbar^3} \sum_{e,e',f} \mu_{e'f} \cdot E_4^*(\omega_{f e'}) \mu_{g e'} \cdot E_3^*(\omega_{e' g}) \\ \times \mu_{ef}^* \cdot E_2(\omega_{f e}) c_i^{e*} \mu_{gi}^* \cdot E_{1,i}^{\text{loc}}(\omega_{eg}) \frac{e^{-i\xi_{f e'} t_3}}{(\Omega_2 - \xi_{f g})(\Omega_1 - \xi_{eg})}$$

and

$$S_{E_{1,ii}}^{\text{loc}}(i, \Omega_1, \Omega_2, t_3) = -\frac{1}{\hbar^3} \sum_{e,e',f} \mu_{g e'} \cdot E_4^*(\omega_{e' g}) \mu_{e' f} \cdot E_3^*(\omega_{f e'}) \\ \times \mu_{ef}^* \cdot E_2(\omega_{f e}) c_i^{e*} \mu_{gi}^* \cdot E_{1,i}^{\text{loc}}(\omega_{eg}) \frac{e^{-i\xi_{e' g} t_3}}{(\Omega_2 - \xi_{f g})(\Omega_1 - \xi_{eg})}.$$

In figure 4(a), we calculated the signal for the localization of the first pulse at different QDs. This leads to a decomposition of the imaginary part obtained for far-field excitation (figure 3(a), right). We can use this information to see which resonance gains contributions from which QD at the ground state to single exciton transition during the first pulse. Since this transition is proportional to the single exciton expansion coefficient $c_i^e \propto S_{E_{1,i}}^{\text{loc}}(i, \Omega_1, \Omega_2, t_3) / (\mu_{gi}^* \cdot E_{1,i}^{\text{loc}}(\omega_{eg}))$, cf equation (14), we can conclude which QD contributes most to which single exciton state. For instance, the resonances at e_2 mainly arise due to the first QD. The single

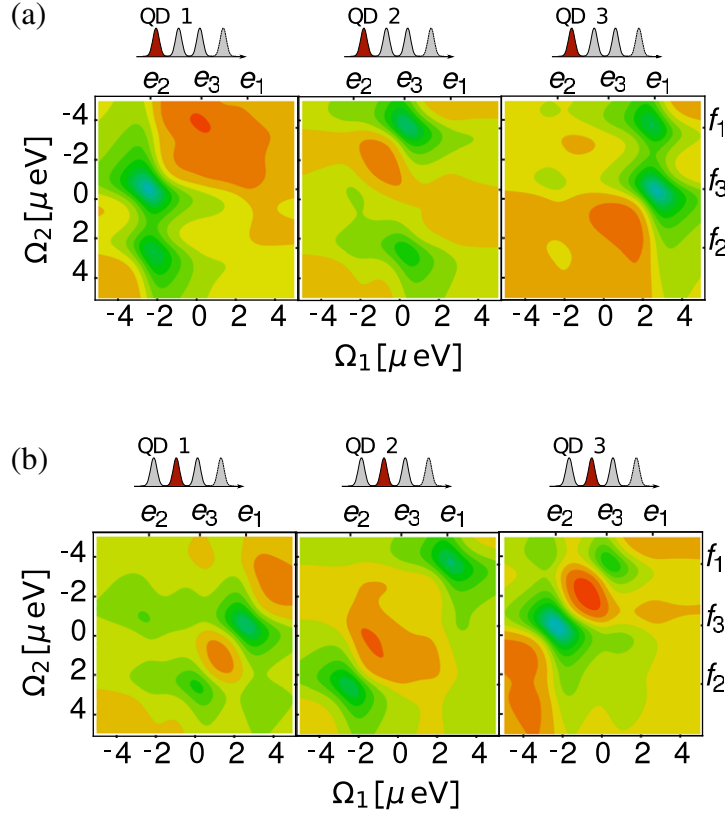


Figure 4. Decomposition of the imaginary part of the DQCS signal with $t_3 = 20$ ps via localization. Part (a) shows spectra with a localized excitation of the first pulse at each QD and part (b) shows a localized second pulse. The detection frequencies are given as detuning around the single and the double gap frequency, respectively.

exciton state e_2 has only optical transitions to f_3 and f_2 . Similarly, the single exciton e_3 arises mostly from QD 2, having two transitions to two excitons, a strong one at f_1 and the smaller one at f_2 . But there are also contributions from the second dot to the exciton state e_2 : a small for the strong resonance with f_3 and a smaller peak connecting e_2 with f_2 .

The single exciton state e_1 is mainly connected to the third QD. State e_1 has strong transitions to f_1 and f_3 . This way, we already gain new information, which would not be possible without localization of the exciting pulses.

3.4. Localization of the first and second pulses

We can also localize the second pulse for the application of our algorithms; therefore we insert for this interaction the local form of the electron light interaction Hamiltonian, equation (13). For the additional localized field at QD j for the second pulse, we use again perfect localization $E_{2,j}^{\text{loc}}(r_l) = E_2^{\text{loc}} \delta_{j,l}$ and obtain

$$S_{E_1, E_2}^{\text{loc}}(i, j, \Omega_1, \Omega_2, t_3) = S_{E_1, E_2, i}^{\text{loc}}(i, j, \Omega_1, \Omega_2, t_3) + S_{E_1, E_2, ii}^{\text{loc}}(i, j, \Omega_1, \Omega_2, t_3) \quad (15)$$

with

$$S_{E_1, E_2, i}^{\text{loc}}(i, j, \Omega_1, \Omega_2, t_3) = \frac{1}{\hbar^3} \sum_{e, e', f} \sum_{k \neq j}^n \mu_{e'f} \cdot E_4^*(\omega_{f e'}) \mu_{g e'} \cdot E_3^*(\omega_{e' g}) \\ \times c_k^e c_{kj}^{f*} \mu_{gj}^* \cdot E_{2,j}^{\text{loc}}(\omega_{f e}) c_i^{e*} \mu_{gi}^* \cdot E_{1,i}^{\text{loc}}(\omega_{e g}) \frac{e^{-i\xi_{f e'} t_3}}{(\Omega_2 - \xi_{f g})(\Omega_1 - \xi_{e g})}$$

and

$$S_{E_1, E_2, ii}^{\text{loc}}(i, j, \Omega_1, \Omega_2, t_3) = -\frac{1}{\hbar^3} \sum_{e, e', f} \sum_{k \neq j}^n \mu_{g e'} \cdot E_4^*(\omega_{e' g}) \mu_{e' f} \cdot E_3^*(\omega_{f e'}) \\ \times c_k^e c_{kj}^{f*} \mu_{gj}^* \cdot E_{2,j}^{\text{loc}}(\omega_{f e}) c_i^{e*} \mu_{gi}^* \cdot E_{1,i}^{\text{loc}}(\omega_{e g}) \frac{e^{-i\xi_{e' g} t_3}}{(\Omega_2 - \xi_{f g})(\Omega_1 - \xi_{e g})},$$

still under the assumption of a localization of the first pulse at QD i .

Using this localization scheme, we can decompose each of the three plots with a localization of the first pulses of figure 4(a) in three plots with also the second pulse localized. In figure 5, we can see the contribution of the QDs to the single exciton to two-exciton transition μ_{ef} , connected to their contribution to the ground state to single exciton transition. If we focus on the case with the first pulse mainly exciting QD 1 (first row), we see that the peak at e_2 with f_3 is mainly visible for a second pulse at QD 3 (and much smaller for a localization at QD 2). On the other hand, with the first pulse mainly exciting QD 3 we see that the peak at e_1 and f_3 is mainly visible for a localization of the second pulse at QD 1. Therefore, we can conclude f_3 that the mainly contributing local two exciton is a state with an excited QD 1 and QD 3. Also the second and the third row show which QD is connected to which single exciton to two-exciton transition of the corresponding spectra of figure 4(a).

In principle, we can see that, in the case of not too strong coupling and thus low delocalization, figure 5 shows from which local single excitons the two excitons $|ij\rangle$ localized at QD i and j are formed.

3.5. Localization of the second pulse

Next, we will show that for reconstructing the two-exciton wave function (see section 3.6.3) it is sufficient to localize the second pulse only. Then, the signal reads

$$S_{E_2}^{\text{loc}}(j, \Omega_1, \Omega_2, t_3) = S_{E_2, i}^{\text{loc}}(j, \Omega_1, \Omega_2, t_3) + S_{E_2, ii}^{\text{loc}}(j, \Omega_1, \Omega_2, t_3) \quad (16)$$

with

$$S_{E_2, i}^{\text{loc}}(j, \Omega_1, \Omega_2, t_3) = \frac{1}{\hbar^3} \sum_{e, e', f} \sum_{k \neq j}^n \mu_{e'f} \cdot E_4^*(\omega_{f e'}) \mu_{g e'} \cdot E_3^*(\omega_{e' g}) \\ \times c_k^e c_{kj}^{f*} \mu_{gj}^* \cdot E_{2,j}^{\text{loc}}(\omega_{f e}) \mu_{ge}^* \cdot E_1(\omega_{e g}) \frac{e^{-i\xi_{f e'} t_3}}{(\Omega_2 - \xi_{f g})(\Omega_1 - \xi_{e g})}$$

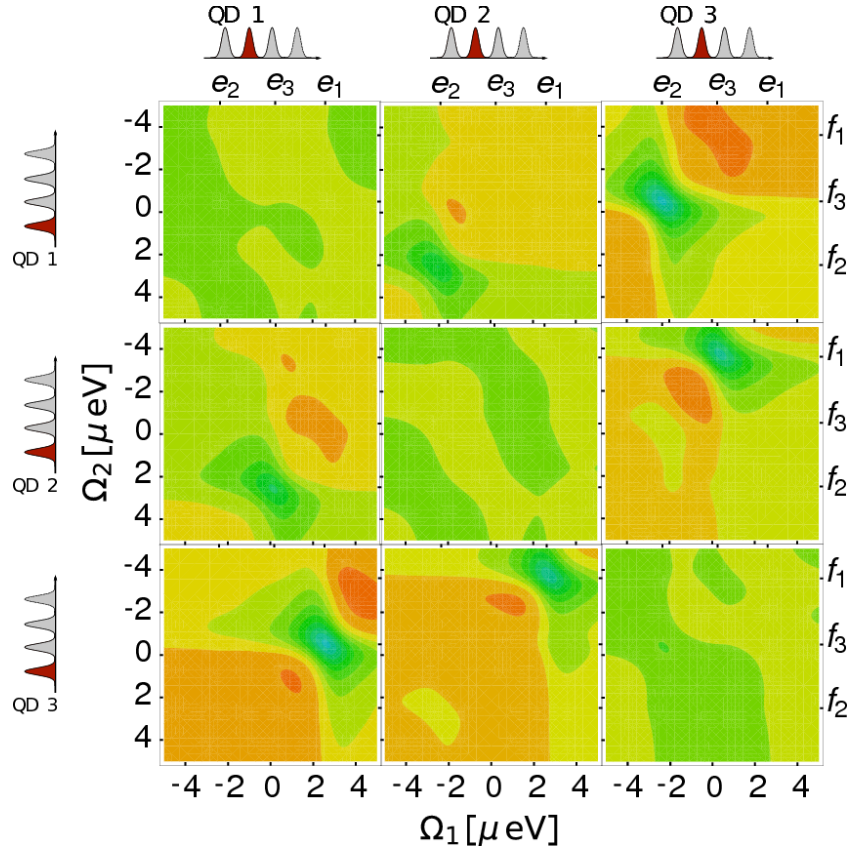


Figure 5. Imaginary part of the localized DQCS signal with $t_3 = 20$ ps with realistic localization. While the rows show which QD is excited by the first pulse, the columns give the QD excited by the second pulse. The spectra can be seen as a decomposition of the imaginary part of the full spectrum in figure 3(a) (right). The detection frequencies are given as detuning around the single and double gap frequencies, respectively.

and

$$S_{E_{2,ii}}^{\text{loc}}(j, \Omega_1, \Omega_2, t_3) = -\frac{1}{\hbar^3} \sum_{e,e',f} \sum_{k \neq j}^n \mu_{ge'} \cdot E_4^*(\omega_{e'g}) \mu_{e'f} \cdot E_3^*(\omega_{fe'}) \\ \times c_k^e c_{kj}^{f*} \mu_{gj}^* \cdot E_{2,j}^{\text{loc}}(\omega_{fe}) \mu_{ge}^* \cdot E_1(\omega_{eg}) \frac{e^{-i\xi_{e'g}t_3}}{(\Omega_2 - \xi_{fg})(\Omega_1 - \xi_{eg})}.$$

The first pulse excites all QDs equally in a far field like the third and fourth pulses.

In figure 4(b), spectra calculated with equation (16) are presented. They represent—opposite to figure 4(a)—the decompositions of the imaginary part using a localization of the second pulse of the far-field spectrum. Here, the two-exciton states cannot be assigned to a certain QD in such a simple way as in the exciton case, since the signal is proportional to $c_k^e c_{kj}^{f*} \mu_{gj}^* \cdot E_{2,j}^{\text{loc}}(\omega_{fe})$ and thus to a product of the single and two-exciton wave

functions. As expected already from the spectrum with two localized pulses, the main part of the resonance at e_2 with f_3 originates from QD 3, whereas the main part of the resonance at e_1 with f_3 originates from QD 1. Thus f_3 is mainly composed of e_1 and e_2 , which are primarily located at QD 3 and QD 1, respectively. In a similar way, we see that f_1 has contributions from e_1 and e_3 mainly localized at QD 2 and QD 3.

3.6. Reconstruction of the wave functions

Localized spectroscopy allows several new applications, since spectroscopic data can be used to obtain more information about coupled nanostructures. In this section, we briefly review a protocol to reconstruct the wave functions of single exciton states, first introduced in [26], and extend this to two-exciton states in coupled nanosystems. Section 3.7 presents a filtering method, which is important for enhancing the algorithms used for the reconstruction and supplements this first introductory section.

If the expansion coefficients c_i^e (single exciton wave functions) and c_{ij}^f (two-exciton wave functions) of equation (2), respectively, are known, it is possible to reconstruct the many particle wave functions $|e\rangle$ and $|f\rangle$. Additionally, the wave functions of the excited state $|i\rangle$ of the isolated emitter i must be known for a full reconstruction. The amplitude and phase of the coefficients c represent how the delocalized wave function is spread over the different QDs. The main idea behind the reconstruction of the wave functions is that spatiotemporal control of electronic fields enables us to eliminate the sum over the QDs i . 2D DQCS, on the other hand, enables us to select specific single and two-exciton states e and f spectrally to remove the summation over e and f . These two techniques allow us to find the coefficients c_i^e for a single exciton state e for QD i and c_{ij}^f for a two-exciton state f for QDs i and j . In the following, we present a calculation and measurement instruction for reconstructing the wave function for a certain single exciton state \bar{e} and a certain two-exciton state \bar{f} .

3.6.1. Single exciton states. In this section, we summarize briefly the method introduced in [26]. For reconstructing the wave function c_i^e , we have to select only the contribution from the spectroscopic signal of a specific single exciton state \bar{e} . We achieve this by extracting the DQCS signal around the frequencies $\Omega_1 \approx \bar{\Omega}_1 \approx \omega_{\bar{e}g}$ and $\Omega_2 \approx \bar{\Omega}_2 \approx \omega_{\bar{f}g}$, where \bar{f} is chosen such that the signal has only a strong contribution connected to \bar{e} . For this, the spectral contributions of other delocalized states are well separated in the DQCS signal from this resonance. Then, the only contributions of the sum over e and f are terms with \bar{e} and \bar{f} . We look at the localized signal for \bar{e} at a fixed time interval T_3 :

$$S_{E_1}^{\text{loc}}(i, \bar{\Omega}_1, \bar{\Omega}_2, T_3) = S_{E_{1,i}}^{\text{loc}}(i, \bar{\Omega}_1, \bar{\Omega}_2, T_3) + S_{E_{1,ii}}^{\text{loc}}(i, \bar{\Omega}_1, \bar{\Omega}_2, T_3) \quad (17)$$

with

$$S_{E_{1,i}}^{\text{loc}}(i, \bar{\Omega}_1, \bar{\Omega}_2, T_3) = \frac{1}{\hbar^3} \sum_{e'} \mu_{e'\bar{f}} \cdot E_4^*(\omega_{\bar{f}e'}) \mu_{ge'} \cdot E_3^*(\omega_{e'g}) \\ \times \mu_{\bar{e}\bar{f}}^* \cdot E_2(\omega_{\bar{f}\bar{e}}) c_i^{\bar{e}*} \mu_{gi}^* \cdot E_{1,i}^{\text{loc}}(\omega_{\bar{e}g}) \frac{e^{-i\xi_{\bar{f}e'}T_3}}{(\bar{\Omega}_2 - \xi_{\bar{f}g})(\bar{\Omega}_1 - \xi_{\bar{e}g})}$$

and

$$S_{E_1,ii}^{\text{loc}}(i, \bar{\Omega}_1, \bar{\Omega}_2, T_3) = -\frac{1}{\hbar^3} \sum_{e'} \mu_{ge'} \cdot E_4^*(\omega_{e'g}) \mu_{e'f} \cdot E_3^*(\omega_{fe'}) \\ \times \mu_{\bar{e}f}^* \cdot E_2(\omega_{f\bar{e}}) c_i^{\bar{e}*} \mu_{gi}^* \cdot E_{1,i}^{\text{loc}}(\omega_{\bar{e}g}) \frac{e^{-i\xi_{e'g}T_3}}{(\bar{\Omega}_2 - \xi_{f\bar{e}})(\bar{\Omega}_1 - \xi_{\bar{e}g})}.$$

The only part of this signal that depends on the selective excitation of QD i is $c_i^{\bar{e}*} \mu_{gi}^* \cdot E_{1,i}^{\text{loc}}(\omega_{\bar{e}g})$. Since both Liouville diagrams share the same interaction at the first step, all other parts do not depend on i . Thus, for the coefficient $c_i^{\bar{e}}$ a proportionality relation⁵ holds:

$$c_i^{\bar{e}*} A = S_{E_1}^{\text{loc}}(i, \bar{\Omega}_1, \bar{\Omega}_2, T_3) / (\mu_{gi}^* \cdot E_{1,i}^{\text{loc}}(\omega_{\bar{e}g})). \quad (18)$$

Assuming that all dipole moments μ_{gi}^* for the single exciton transitions and the localized field $E_{1,i}^{\text{loc}}(\omega_{\bar{e}g})$ are known, we can extract from equation (18) all coefficients $c_i^{\bar{e}*}$ except for a proportionality factor A . From the normalization of the wave functions we find that $\sum_i^n |c_i^{\bar{e}}|^2 = 1$, so that the coefficient can be determined (except for an arbitrary phase) and the three wave function coefficients are thus reconstructed. To **summarize** the method for reconstructing the single exciton wave function, we need as **input information** the dipole moments μ_{gi} for all QDs i . In the **measurement**, we first select frequencies $\bar{\Omega}_1$ and $\bar{\Omega}_2$ with a main contribution by the single exciton state \bar{e} to be reconstructed. Then DQCS signal $S_{E_1}^{\text{loc}}(i, \bar{\Omega}_1, \bar{\Omega}_2, T_3)$ is recorded for all QDs i . In **postprocessing** the expansion coefficient of the exciton wave function $c_i^{\bar{e}}$ are obtained $c_i^{\bar{e}} = S_{E_1}^{\text{loc}}(i, \bar{\Omega}_1, \bar{\Omega}_2, T_3) / (\mu_{gi}^* \cdot E_{1,i}^{\text{loc}}(\omega_{\bar{e}g}) A)$, where A is found by the normalization of the wave function $|\bar{e}\rangle$: $\sum_i |c_i^{\bar{e}}|^2$.

3.6.2. Determining and enhancing the quality of the reconstructed single exciton states. In table 1, all original single exciton states that belong to the chosen example can be compared with the reconstructed values. We find that e_1 is the state with the best reconstruction. Furthermore, the best reconstruction is reached choosing the energy of the two-excitonic state f_3 to ground state transition for Ω_2 . This is because that peak has the lowest influence from other resonances (cf the spectrum in figure 3(a)). For the same reason, we choose for the reconstruction of e_2 the resonance with f_3 and of e_3 the resonance with f_1 .

We measured the quality in terms of the squared error $\sqrt{\sum_{i=1}^n \|c_i^{\text{rec}}\|^2 - |c_i^{\text{org}}|^2}$ of the difference of the original wave function coefficient c_i^{org} and the reconstructed one c_i^{rec} . This way of error determination does not consider the phase, but it has the most physical meaning since the square of the coefficient gives information about the occupation probability.⁶

We can still improve the quality of reconstruction of $c_i^{e_1}$ by moving the measurement point spectrally in the direction of higher single exciton energies, since then we decrease the influence of other resonances.⁷ This works well mostly except for reconstructing state e_2 . Also, one would assume that moving the measurement point in the negative Ω_1

⁵ Note: although we assumed a Lorentzian broadening in our equations, this proportionality should not depend on this choice.

⁶ Reconstructed after filtering states e_1 and e_2

⁷ The measurement points located near the resonance peak (shifted for better reconstruction) is given via $\omega_{e_1g} = 2.60 \mu\text{eV}$ ($\omega_{e_1g} = 3.12 \mu\text{eV}$), $\omega_{e_2g} = -2.35 \mu\text{eV}$ ($\omega_{e_2g} = -3.20 \mu\text{eV}$) and $\omega_{e_3g} = 0.25 \mu\text{eV}$. For the corresponding two-exciton measurement points we have $\omega_{f_1g} = 3.60 \mu\text{eV}$ and $\omega_{f_3g} = 0.49 \mu\text{eV}$.

Table 1. Comparison of the original (O) with the reconstructed (R) single exciton wave function coefficients for a shifted measurement point using a perfect localization: The phase is written in multiples of 2π . The error is calculated via $\sqrt{\sum_{i=1}^n \|c_i^{\text{rec}}\|^2 - \|c_i^{\text{org}}\|^2}$. Additionally, the results of a measurement point at the center of the resonance are given (C). A reconstruction after filtering e_2 is marked with (F) and a reconstruction after filtering states e_1 and e_2 (FF).

State	Type	$ c_1^e $	$ c_2^e $	$ c_3^e $	$\arg(c_1^e)$	$\arg(c_2^e)$	$\arg(c_3^e)$	Error
e_1	O	0.115	0.104	0.988	0.500	0.500	0.000	
	R	0.205	0.081	0.975	0.414	0.190	0.710	0.04
	C	0.247	0.077	0.966	0.433	0.281	0.787	0.06
e_2	O	0.977	0.169	0.131	0.500	0.500	0.500	
	R	0.949	0.110	0.294	0.836	0.820	0.952	0.09
	F	0.969	0.138	0.205	0.845	0.858	0.650	0.03
	C	0.969	0.136	0.206	0.725	0.680	0.907	0.03
e_3	O	0.180	0.980	0.083	0.000	0.500	0.500	
	R	0.360	0.858	0.366	0.342	0.792	0.903	0.28
	F	0.381	0.920	0.093	0.316	0.794	0.968	0.16
	FF	0.138	0.987	0.081	0.302	0.796	0.873	0.02

direction improves the reconstruction quality. But in this special case, interferences of positive and negative contributions are destructive on the right-hand side of the strong peak (e_2 , f_3) and so the influence of other resonances decreases moving to higher energies. Another idea for increasing the quality of reconstruction is averaging over an area of measurement points or additional weighting the results with a Gaussian centered at the main resonance peak; however, this is beyond the scope of this paper. Additionally, we compared in table 1 the reconstruction for choosing Ω_1 , Ω_2 at the center of the resonances.

Reconstructing the exciton wave functions shows overall good agreement for both the amplitude and the relative phase. The values of the resonance with the highest oscillator strength are exemplary illustrated in figure 6.

3.6.3. Two-exciton states. Similar to the procedure for single excitons, the two-exciton wave functions can also be reconstructed. As a prerequisite, the single exciton reconstruction has to be completed and c_i^e must be known for all single excitons (except for a global phase factor) connected to the two-exciton state.

Here, we use the signal with a localized second pulsed (equation (16)). We select a single exciton state \bar{e} and a two-exciton state \bar{f} ; then $S_{E_2}^{\text{loc}}(j, \bar{e}, \bar{f}, T_3)$ is the signal with localized second pulses evaluated for frequencies $\bar{\Omega}_1$ and $\bar{\Omega}_2$ for which mainly \bar{e} and \bar{f} contribute ($\bar{\Omega}_1 \approx \omega_{\bar{e}g}$ and $\bar{\Omega}_2 \approx \omega_{\bar{f}\bar{e}}$). We start with rewriting the signal with localized second pulse (equation (16)) just

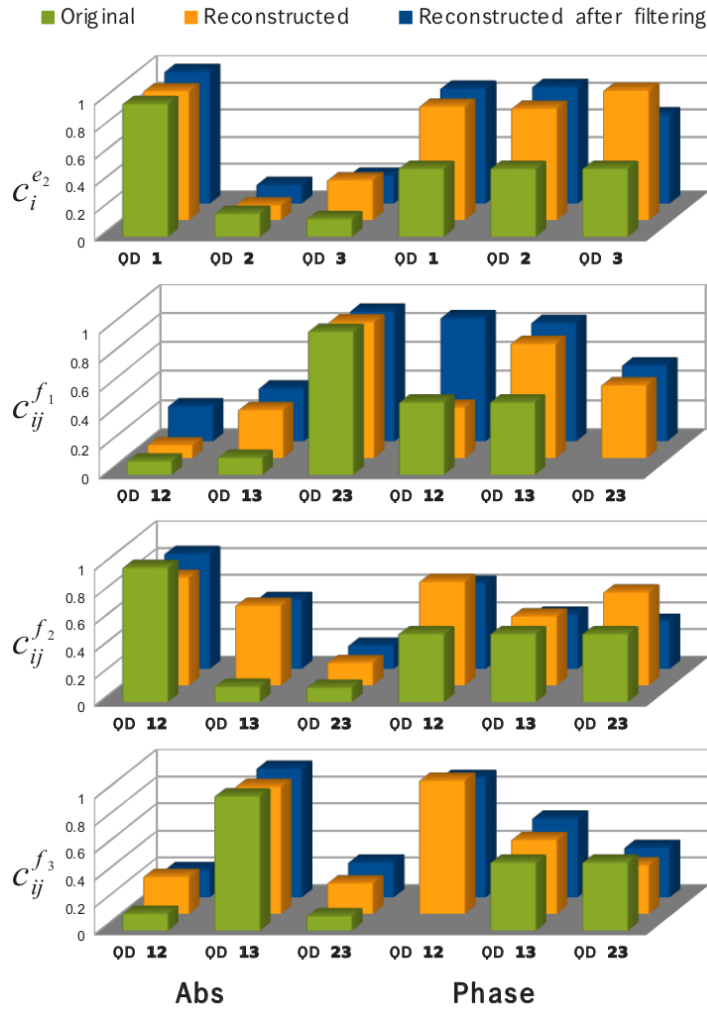


Figure 6. Coefficients for reconstructing the wave function for the states with a high oscillator strength: above, the original and the reconstructed state with and without filtering of $c_i^{e_2}$ are presented, whereas below, the original and the reconstructed two-exciton wave function coefficients are shown. Filtering shows a small improvement here.

for one selected single exciton state \bar{e} and one selected two-exciton state \bar{f} as explained in section 3.6.1 and obtain

$$S_{E_2}^{\text{loc}}(j, \bar{e}, \bar{f}, T_3) = S_{E_{2,i}}^{\text{loc}}(j, \bar{e}, \bar{f}, T_3) + S_{E_{2,ii}}^{\text{loc}}(j, \bar{e}, \bar{f}, T_3)$$

with

$$S_{E_{2,i}}^{\text{loc}}(j, \bar{e}, \bar{f}, T_3) = \frac{1}{\hbar^3} \sum_{e'} \sum_{k \neq j}^n \mu_{e' \bar{f}} \cdot E_4^*(\omega_{\bar{f}e'}) \mu_{ge'} \cdot E_3^*(\omega_{e'g}) \\ \times c_k^{\bar{e}} c_{kj}^{\bar{f}*} \mu_{gj}^* \cdot E_2^{\text{loc}}(\omega_{\bar{f}\bar{e}}) \mu_{g\bar{e}}^* \cdot E_1(\omega_{\bar{e}g}) \frac{e^{-i\xi_{\bar{f}e'} T_3}}{(\bar{\Omega}_2 - \xi_{\bar{f}g})(\bar{\Omega}_1 - \xi_{\bar{e}g})}$$

and

$$S_{E_2,ii}^{\text{loc}}(j, \bar{e}, \bar{f}, T_3) = -\frac{1}{\hbar^3} \sum_{e'} \sum_{k \neq j}^n \mu_{ge'} \cdot E_4^*(\omega_{e'g}) \mu_{e'\bar{f}} \cdot E_3^*(\omega_{\bar{f}e'}) \\ \times c_k^{\bar{e}} c_{kj}^{\bar{f}*} \mu_{gj}^* \cdot E_2^{\text{loc}}(\omega_{\bar{f}\bar{e}}) \mu_{g\bar{e}}^* \cdot E_1(\omega_{\bar{e}g}) \frac{e^{-i\xi_{e'g}T_3}}{(\bar{\Omega}_2 - \xi_{\bar{f}g})(\bar{\Omega}_1 - \xi_{\bar{e}g})}.$$

We can use the appearance of the factors $c_k^{\bar{e}} c_{kj}^{\bar{f}*} \mu_{gj}^* \cdot E_2^{\text{loc}}(\omega_{\bar{f}\bar{e}})$ in the signal as the starting point for being able to derive an equation analogous to equation (18) for the extraction of two-exciton wave functions. We can reformulate this by introducing proportionality factors $B_{\bar{e}}^{\bar{f}}$, which do not depend on localization:

$$\sum_{k \neq j}^n c_k^{\bar{e}} c_{kj}^{\bar{f}*} B_{\bar{e}}^{\bar{f}} = S_{E_2}^{\text{loc}}(j, \bar{e}, \bar{f}, T_3) / (\mu_{gj}^* \cdot E_2^{\text{loc}}(\omega_{\bar{f}\bar{e}})). \quad (19)$$

Here, the factor $B_{\bar{e}}^{\bar{f}}$ combines all parts that do not depend on k or j ; the form of equation (19) should again not depend on the dephasing model. But as a substantial difference to the single exciton case, we have several factors $B_{\bar{e}}^{\bar{f}}$ multiplied with single and two-exciton wave function coefficients under a sum over k and j .

Therefore, the next step for isolating the two-exciton wave function $c_{kj}^{\bar{f}*}$ would be isolating the single exciton wave function $c_k^{\bar{e}}$ on the left-hand side of equation (19). But we have to recognize that the other factors $B_{\bar{e}}^{\bar{f}}$ and $c_{kj}^{\bar{f}*}$ depend also on the single and two-exciton states, so we cannot apply the orthogonality relation like in the single exciton case. Dividing by $B_{\bar{e}}^{\bar{f}}$ before applying the orthogonality relation is no alternative, since these factors are unknown and should consequently not appear on the right-hand side. Instead of calculating $B_{\bar{e}}^{\bar{f}}$ for every e' , we compute the ratio of the factor of two arbitrary exciton states: for this we multiply equation (19) with $c_j^{\bar{e}}$ and sum over j and obtain

$$\sum_{j, k \neq j}^n c_k^{\bar{e}} c_j^{\bar{e}} c_{kj}^{\bar{f}*} B_{\bar{e}}^{\bar{f}} = \sum_j^n c_j^{\bar{e}} S_{E_2}^{\text{loc}}(j, \bar{e}, \bar{f}, T_3) / (\mu_{gj}^* \cdot E_2^{\text{loc}}(\omega_{\bar{f}\bar{e}})).$$

Exchanging \bar{e} and \tilde{e} and the index k with j on the left-hand side and using that $c_{kj}^{\bar{f}*} = c_{jk}^{\bar{f}*}$ yields

$$\sum_{j, k \neq j}^n c_j^{\bar{e}} c_k^{\bar{e}} c_{kj}^{\bar{f}*} B_{\bar{e}}^{\bar{f}} = \sum_j^n c_j^{\bar{e}} S_{E_2}^{\text{loc}}(j, \tilde{e}, \bar{f}, T_3) / (\mu_{gj}^* \cdot E_2^{\text{loc}}(\omega_{\bar{f}\bar{e}})),$$

so that by dividing the two equations we obtain the ratio

$$B_{\bar{e}}^{\bar{f}} / B_{\tilde{e}}^{\bar{f}} = \sum_j^n c_j^{\tilde{e}} / c_j^{\bar{e}} \cdot S_{E_2}^{\text{loc}}(j, \bar{e}, \bar{f}, T_3) / S_{E_2}^{\text{loc}}(j, \tilde{e}, \bar{f}, T_3). \quad (20)$$

This is the first ingredient in the reconstruction, which can be calculated by the measured or derived quantities for each combination of two arbitrary single exciton states \bar{e} and \tilde{e} . In order

to remove factors $B_{\bar{e}}^{\bar{f}}$ on the left side, we choose again another arbitrary exciton state \hat{e} and multiply equation (19) by $B_{\hat{e}}^{\bar{f}}$ and divide by $B_{\bar{e}}^{\bar{f}}$ to obtain

$$\sum_{k \neq j}^n c_{\bar{e}k}^{\bar{f}*} c_{kj}^{\bar{f}} B_{\bar{e}}^{\bar{f}} = S_{E_2}^{\text{loc}}(j, \bar{e}, \bar{f}, T_3) / (\mu_{gj}^* \cdot E_{2,j}^{\text{loc}}(\omega_{\bar{f}\bar{e}})) \cdot B_{\hat{e}}^{\bar{f}} / B_{\bar{e}}^{\bar{f}}. \quad (21)$$

Here the complete right side of equation (21) is known; one contribution is the measurable spectrum, the single exciton coefficients and the ratio $B_{\hat{e}}^{\bar{f}} / B_{\bar{e}}^{\bar{f}}$, which can be calculated using the measured data and equation (20).

Since $B_{\hat{e}}^{\bar{f}}$ does not depend on \bar{e} , we can now calculate the two-exciton wave function by multiplying equation (21) with $c_i^{\bar{e}*}$ and summing over \bar{e} . This leads to an orthogonality relation and we obtain

$$c_{ij}^{\bar{f}*} B_{\hat{e}}^{\bar{f}} = \sum_{\bar{e}} c_i^{\bar{e}*} S_{E_2}^{\text{loc}}(j, \bar{e}, \bar{f}, T_3) / (\mu_{gj}^* \cdot E_{2,j}^{\text{loc}}(\omega_{\bar{f}\bar{e}})) \cdot B_{\hat{e}}^{\bar{f}} / B_{\bar{e}}^{\bar{f}}.$$

We can now use that the expansion coefficients have been normalized and use $\sum_{i,j < i}^n |c_{ij}^{\bar{f}}|^2 = 1$ to obtain the two-exciton wave functions of coupled QDs.

After deriving the procedure, we **summarize** the steps necessary for the reconstruction. As **input information** we need the dipole moments matrix elements μ_{gi} for all QDs i and the single excitonic wave function coefficients c_i^e for all single exciton states. As **measurement** the DQCS signal with a localized second pulse at QD j $S_{E_2}^{\text{loc}}(j, \bar{e}, \bar{f}, T_3)$ has to be recorded. In **postprocessing**, we first calculate the ratios $B_{\hat{e}}^{\bar{f}} / B_{\bar{e}}^{\bar{f}} = \sum_j^n c_j^{\bar{e}} / c_j^{\bar{e}} \cdot S_{E_2}^{\text{loc}}(j, \bar{e}, \bar{f}, T_3) / S_{E_2}^{\text{loc}}(j, \bar{e}, \bar{f}, T_3)$ for all combinations of single exciton states. Then $c_{ij}^{\bar{f}}$ is calculated via $c_{ij}^{\bar{f}} B_{\hat{e}}^{\bar{f}} = \sum_{\bar{e}} c_i^{\bar{e}*} S_{E_2}^{\text{loc}}(j, \bar{e}, \bar{f}, T_3) / (\mu_{gj}^* \cdot E_{2,j}^{\text{loc}}(\omega_{\bar{f}\bar{e}})) \cdot B_{\hat{e}}^{\bar{f}} / B_{\bar{e}}^{\bar{f}}$. Afterwards $c_{ij}^{\bar{f}} B_{\hat{e}}^{\bar{f}}$ is normalized, using the two-exciton wave function normalization condition $|B_{\hat{e}}^{\bar{f}}|^2 = \sum_{ij} |c_{ij}^{\bar{f}} B_{\hat{e}}^{\bar{f}}|^2$. So that we can calculate $c_{ij}^{\bar{f}}$ up to a global phase.

The results of reconstructing the two-exciton wave functions are shown in table 2. An illustration can be found in figure 6. Again, original states and reconstructed values agree, but not as well as for the exciton state. We can always determine which local two-exciton states contribute most to the delocalized two-exciton state. But crosstalk between the different resonances makes it difficult (cf the reconstruction for f_1) to determine the quantitative contribution of the less contributing local two-exciton states, whereas for the other two two-exciton states the agreement is much more acceptable.

The overall reason for this is that the two-exciton wave functions are calculated using the single exciton wave functions: the errors in obtaining the single exciton wave function are cumulated in the two-exciton wave function. Furthermore, for the reconstruction of the two-exciton wave function the spectrum localized at the second pulse enters not only for one combination of Ω_1 and Ω_2 but for every single exciton; this also increases the possible errors. This leads to an overall reduced quality of the reconstructed two-exciton wave function.

3.7. Filtering different resonances

In [26], it was shown that a 2D spectrum with the first pulses localized allows to remove certain resonances using postprocessing of the spectra. Since most of the errors in the reconstruction is caused by overlapping resonances, this might enhance the reconstruction of the exciton states.

Table 2. Comparison of the original (O) with the reconstructed two-exciton wave function coefficients for a shifted measurement point in (R). The data marked with (F) uses filtered spectra for the reconstruction. Additionally, the results of a measurement point at the center of the resonance for all single exciton states are given (C). For all calculations a perfect localization was assumed. The phase is written in multiples of 2π .

State	Type	$ c_{12}^f $	$ c_{13}^f $	$ c_{23}^f $	$\varphi(c_{12}^f)$	$\varphi(c_{13}^f)$	$\varphi(c_{23}^f)$	Error
f_1	O	0.093	0.118	0.989	0.500	0.500	0.000	
	R	0.089	0.332	0.939	0.349	0.789	0.503	0.14
	F	0.244	0.367	0.898	0.852	0.819	0.525	0.22
	C	0.140	0.377	0.915	0.313	0.709	0.424	0.19
f_2	O	0.988	0.113	0.106	0.500	0.500	0.500	
	R	0.793	0.586	0.166	0.762	0.508	0.684	0.48
	F	0.845	0.507	0.171	0.628	0.400	0.347	0.36
	C	0.778	0.601	0.184	0.705	0.424	0.257	0.51
f_3	O	0.124	0.987	0.106	0.000	0.500	0.500	
	R	0.273	0.935	0.225	0.981	0.544	0.358	0.12
	F	0.201	0.946	0.256	0.879	0.580	0.364	0.10
	C	0.297	0.921	0.253	0.879	0.464	0.270	0.15

We will recapitulate the procedure, modified for the extraction process of the coefficients. For this, we note that the spectra equations (14), (16) and (15) have the form of a sum over individual contributions h_e for different exciton states e :

$$\begin{aligned}
 S_{E_1}^{\text{loc}}(i, \Omega_1, \Omega_2, t_3) &= \sum_e c_i^{e*} \mu_{gi}^* \cdot E_{1,i}^{\text{loc}}(\omega_{eg}) h_e(\Omega_1, \Omega_2, t_3), \\
 S_{\varphi_{\text{III}}}^{(3)}(\Omega_1, \Omega_2, t_3) &= \sum_e c_i^{e*} \mu_{gi}^* \cdot E_{1,i}^{\text{loc}}(\omega_{eg}) h_e(\Omega_1, \Omega_2, t_3), \\
 S_{E_1, E_2}^{\text{loc}}(i, j, \Omega_1, \Omega_2, t_3) &= \sum_e c_i^{e*} \mu_{gi}^* \cdot E_{1,i}^{\text{loc}}(\omega_{eg}) h_e(j, \Omega_1, \Omega_2, t_3), \\
 S_{E_2}^{\text{loc}}(j, \Omega_1, \Omega_2, t_3) &= \sum_e c_i^{e*} \mu_{gi}^* \cdot E_{1,i}^{\text{loc}}(\omega_{eg}) h_e(j, \Omega_1, \Omega_2, t_3), \tag{22}
 \end{aligned}$$

where the functions h_e can be calculated from the measured 2D spectrum:

$$\begin{aligned}
 h_{\bar{e}}(\Omega_1, \Omega_2, t_3) &= \sum_i^n c_i^{\bar{e}} S_{E_1}^{\text{loc}}(i, \Omega_1, \Omega_2, t_3) / (\mu_{gi}^* \cdot E_{1,i}^{\text{loc}}(\omega_{eg})), \\
 h_{\bar{e}}(j, \Omega_1, \Omega_2, t_3) &= \sum_i^n c_i^{\bar{e}} S_{E_1, E_2}^{\text{loc}}(i, j, \Omega_1, \Omega_2, t_3) / (\mu_{gi}^* \cdot E_{1,i}^{\text{loc}}(\omega_{eg})). \tag{23}
 \end{aligned}$$

In the construction of $h_{\bar{e}}$, we exploited a scalar product, which was constructed by multiplying equation (22) with $c_i^{\bar{e}*}$ and summing over i and using the orthogonality of the delocalized states.

Using this formula, we can filter in postprocessing all resonances to which a certain ground state g to single exciton \bar{e} transition contributes during the first pulse. The filtered spectra can be calculated as

$$\begin{aligned} S_{E_1}^{\text{filter,loc}}(\bar{e}, i, \Omega_1, \Omega_2, t_3) &= S_{E_1}^{\text{loc}}(i, \Omega_1, \Omega_2, t_3) - c_i^{\bar{e}*} \mu_{gi}^* \cdot E_{1,i}^{\text{loc}}(\omega_{eg}) h_{\bar{e}}(i, \Omega_1, \Omega_2, t_3) \\ &= \sum_{e \neq \bar{e}} c_i^{e*} \mu_{gi}^* \cdot E_{1,i}^{\text{loc}}(\omega_{eg}) h_e(\Omega_1, \Omega_2, t_3), \end{aligned} \quad (24)$$

$$\begin{aligned} S_{\varphi_{\text{III}}}^{\text{filter}}(\bar{e}, \Omega_1, \Omega_2, t_3) &= S_{\varphi_{\text{III}}}^{(3)}(\Omega_1, \Omega_2, t_3) - \sum_i c_i^{\bar{e}*} \mu_{gi}^* \cdot E_{1,i}^{\text{loc}}(\omega_{eg}) h_{\bar{e}}(\Omega_1, \Omega_2, t_3) \\ &= \sum_{e \neq \bar{e}} c_i^{e*} \mu_{gi}^* \cdot E_{1,i}^{\text{loc}}(\omega_{eg}) h_e(\Omega_1, \Omega_2, t_3), \end{aligned} \quad (25)$$

$$\begin{aligned} S_{E_1, E_2}^{\text{filter,loc}}(\bar{e}, i, j, \Omega_1, \Omega_2, t_3) &= S_{E_1, E_2}^{\text{loc}}(i, j, \Omega_1, \Omega_2, t_3) - c_i^{\bar{e}*} \mu_{gi}^* \cdot E_{1,i}^{\text{loc}}(\omega_{eg}) h_{\bar{e}}(j, \Omega_1, \Omega_2, t_3) \\ &= \sum_{e \neq \bar{e}} c_i^{e*} \mu_{gi}^* \cdot E_{1,i}^{\text{loc}}(\omega_{eg}) h_e(j, \Omega_1, \Omega_2, t_3), \end{aligned} \quad (26)$$

$$\begin{aligned} S_{E_2}^{\text{filter,loc}}(j, \Omega_1, \Omega_2, t_3) &= S_{E_2}^{\text{loc}}(\bar{e}, j, \Omega_1, \Omega_2, t_3) - \sum_i c_i^{\bar{e}*} \mu_{gi}^* \cdot E_{1,i}^{\text{loc}}(\omega_{eg}) h_{\bar{e}}(j, \Omega_1, \Omega_2, t_3) \\ &= \sum_{e \neq \bar{e}} c_i^{e*} \mu_{gi}^* \cdot E_{1,i}^{\text{loc}}(\omega_{eg}) h_e(j, \Omega_1, \Omega_2, t_3). \end{aligned} \quad (27)$$

In figure 3(b), for each resonance a filtered spectrum is presented; we can clearly see that the corresponding resonances are removed from spectra. Therefore it is expected that using the filtered version (out filtering of the already reconstructed states) of the spectrum can clearly enhance further reconstruction of exciton states.

Here, we try to investigate if the filtered spectrum is improving the quality of the reconstructed coefficients. The filtering improves the quality of the reconstructed wave function as can be seen from the error rates for the reconstructed wave function using a filtered spectrum in tables 1 and 2.

As discussed in section 3.6.1, we find the best reconstruction for e_1 and the second best for e_2 , since e_1 dominates the spectrum. This is the reason why we used, while reconstructing the exciton state e_2 , a spectrum with filtering the state e_1 out. For the exciton state e_3 we filter two states, since the states e_1 and e_2 are now known. We do not get better values for every single QD, but there is still an overall improvement visible. The results show that filtering can reduce the error of the reconstruction of single excitons (see table 1) at least by a factor of 2 and in the case of the weak resonance e_3 by an order of magnitude.

Since one can determine all exciton states, filtering all the single exciton states is possible for reconstructing the two-exciton states. Again, the filtering technique supplies results for most coefficients at a higher quality as can be seen in table 2. But the improvement is not as high as in the case of single excitons, since we have no available filtering for the two-exciton part.

4. Applicability of the reconstruction

The presented methods are not limited to the example of coupled self-organized GaAs/InAs dots. In principle, they are applicable to any system of coupled emitters with two dominant

levels contributing to the optical response describable by the Hamiltonian from equation (1). Such systems include colloidal QDs, coupled chromophores, J-aggregates, plasmons in coupled metal nanoparticles, as long as a suitable spatial localization technique for optical fields exists. In order to form the detuning of the individual emitter transition frequency should be smaller or the same order of magnitude as the dipole–dipole coupling—but big enough to separate exciton states.

Additionally, prerequisites apply to the couplings; the dipole couplings between the emitters should be greater than the linewidth of the resonances (dephasing time) in order to be able to separate the delocalized states in frequency space.

Generalization to emitters with more than two levels is possible although the accessible properties might be reduced.

5. Conclusion

In conclusion, we can reconstruct delocalized exciton wave functions of coupled QDs by finding the expansion coefficients of the basis representation. Single particle wave functions of one QD serve as the basis for the single exciton states and two-exciton states serve as two-exciton basis. These prefactors are found with the help of localized spectroscopy.

We have presented protocols for reconstructing delocalized wave functions for exciton states as well as for two-exciton states. The quality of reconstruction depends among other factors on the quality of spatiotemporal control and on influences of neighbor resonances in the frequency domain. Filtering methods can, furthermore, reduce unwanted influences of resonances and thus improve the quality of reconstruction.

Acknowledgments

We gratefully acknowledge support from the Deutsche Forschungsgemeinschaft (DFG) through SPP 1391 (MR and FeS) and SFB 910 (AK). MR also acknowledges support from the Alexander von Humboldt Foundation through the Feodor-Lynen program. SM gratefully acknowledges support from NSF grant CHE-1058791, DARPA BAA-10-40 QUBE and the Chemical Sciences, Geosciences and Biosciences Division, Office of Basic Energy Sciences, Office of Science, (US) Department of Energy (DOE).

References

- [1] Guenther T, Lienau C, Elsaesser T, Glanemann M, Axt V M, Kuhn T, Eshlaghi S and Wieck A D 2002 Coherent nonlinear optical response of single quantum dots studied by ultrafast near-field spectroscopy *Phys. Rev. Lett.* **89** 057401
- [2] Lovett B W, Reina J H, Nazir A and Briggs G A D 2003 Optical schemes for quantum computation in quantum dot molecules *Phys. Rev. B* **68** 205319
- [3] Engel G S, Calhoun T R, Read E L, Ahn T-K, Mancal T, Cheng Y-C, Blankenship R E and Fleming G R 2007 Evidence for wavelike energy transfer through quantum coherence in photosynthetic systems *Nature* **446** 782–6
- [4] Christensson N, Milota F, Nemeth A, Pugliesi I, Riedle E, Sperling J, Pullerits T, Kauffmann H F and Hauer J 2010 Electronic double-quantum coherences and their impact on ultrafast spectroscopy: the example of β -carotene *J. Phys. Chem. Lett.* **1** 3366–70

- [5] Carmele A, Knorr A and Richter M 2009 Photon statistics as a probe for exciton correlations in coupled nanostructures *Phys. Rev. B* **79** 035316
- [6] Danckwerts J, Ahn K J, Förstner J and Knorr A 2006 Theory of ultrafast nonlinear optics of Coulomb-coupled semiconductor quantum dots: Rabi oscillations and pump–probe spectra *Phys. Rev. B* **73** 165318
- [7] De Wit A (ed) 2011 *22nd Solvay Conf. on Chemistry; Procedia Chem.* **3** 1–366
- [8] Dachner M-R *et al* 2010 Theory of carrier and photon dynamics in quantum dot light emitters *Phys. Status Solidi b* **247** 809–28
- [9] Malic E, Weber C, Richter M, Atalla V, Klamroth T, Saalfrank P, Reich S and Knorr A 2011 Microscopic model of the optical absorption of carbon nanotubes functionalized with molecular spiropyran photoswitches *Phys. Rev. Lett.* **106** 097401
- [10] Schoth M, Richter M, Knorr A and Renger T 2012 Line narrowing of excited-state transitions in nonlinear polarization spectroscopy: application to water–soluble chlorophyll–binding protein *Phys. Rev. Lett.* **108** 178104
- [11] Aeschlimann M, Bauer M, Bayer D, Brixner T, Javier Garcia, de Abajo F, Pfeiffer W, Rohmer M, Spindler C and Steeb F 2007 Adaptive subwavelength control of nano-optical fields *Nature* **446** 301–4
- [12] Brixner T, García de Abajo F J, Schneider J and Pfeiffer W 2005 Nanoscopic ultrafast space-time-resolved spectroscopy *Phys. Rev. Lett.* **95** 093901
- [13] Aeschlimann M *et al* 2010 Spatiotemporal control of nanooptical excitations *Proc. Natl Acad. Sci. USA* **107** 5329–33
- [14] Aeschlimann M, Brixner T, Fischer A, Kramer C, Melchior P, Pfeiffer W, Schneider C, Strüber C, Tuchscherer P and Voronine D V 2011 Coherent two-dimensional nanoscopy *Science* **333** 1723–6
- [15] von Freymann G, Schimmel Th, Wegener M, Hanewinkel B, Knorr A and Koch S W 1998 Computer simulations on near-field scanning optical microscopy: can subwavelength resolution be obtained using uncoated optical fiber probes? *Appl. Phys. Lett.* **73** 1170–2
- [16] Pettinger B, Ren B, Picardi G, Schuster R and Ertl G 2004 Nanoscale probing of adsorbed species by tip-enhanced raman spectroscopy *Phys. Rev. Lett.* **92** 096101
- [17] Weber-Bargioni A *et al* 2011 Hyperspectral nanoscale imaging on dielectric substrates with coaxial optical antenna scan probes *Nano Lett.* **11** 1201–7
- [18] Zhang Z, Weber-Bargioni A, Wu S W, Dhuey S, Cabrini S and Schuck P J 2009 Manipulating nanoscale light fields with the asymmetric bowtie nano-colorsorter *Nano Lett.* **9** 4505–9
- [19] Kinkhabwala A, Yu Z, Fan S, Avlasevich Y, Mullen K and Moerner W E 2009 Large single-molecule fluorescence enhancements produced by a bowtie nanoantenna *Nature Photon.* **3** 654–7
- [20] Huang J S, Voronine D V, Tuchscherer P, Brixner T and Hecht B 2009 Deterministic spatiotemporal control of optical fields in nanoantennas and plasmonic circuits *Phys. Rev. B* **79** 195441
- [21] Merlein J, Kahl M, Zuschlag A, Sell A, Halm A, Boneberg J, Leiderer P, Leitenstorfer A and Bratschitsch R 2008 Nanomechanical control of an optical antenna *Nature Photon.* **2** 230–3
- [22] Novotny L and van Hulst N 2011 Antennas for light *Nature Photon.* **5** 83–90
- [23] Schuller J A, Barnard E S, Cai W, Jun Y C, White J S and Brongersma M L 2010 Plasmonics for extreme light concentration and manipulation *Nature Mater.* **9** 193–204
- [24] Abramavicius D, Palmieri B, Voronine D V, Sanda F and Mukamel S 2009 Coherent multidimensional optical spectroscopy of excitons in molecular aggregates; quasiparticle versus supermolecule perspectives *Chem. Rev.* **109** 2350–408
- [25] Tian P, Keusters D, Suzuki Y and Warren W S 2003 Femtosecond phase-coherent two-dimensional spectroscopy *Science* **300** 1553–5
- [26] Richter M, Schlosser F, Schoth M, Burger S, Schmidt F, Knorr A and Mukamel S 2012 Reconstruction of the wave functions of coupled nanoscopic emitters using a coherent optical technique *Phys. Rev. B* **86** 085308
- [27] Stone K W, Gundogdu K, Turner D B, Li X, Cundiff S T and Nelson K A 2009 Two-quantum 2D FT electronic spectroscopy of biexcitons in GaAs quantum wells *Science* **324** 1169–73

- [28] Karaiskaj D, Bristow A D, Yang L, Dai X, Mirin R P, Mukamel S and Cundiff S T 2010 Two-quantum many-body coherences in two-dimensional Fourier-transform spectra of exciton resonances in semiconductor quantum wells *Phys. Rev. Lett.* **104** 117401
- [29] Mukamel S 1995 *Principles of Nonlinear Optical Spectroscopy* (New York: Oxford University Press)
- [30] Keusters D, Tan H-S and Warren W S 1999 Role of pulse phase and direction in two-dimensional optical spectroscopy *J. Phys. Chem. A* **103** 10369–80
- [31] Brixner T, Mančal T, Stiopkin I V and Fleming G R 2004 Phase-stabilized two-dimensional electronic spectroscopy *J. Chem. Phys.* **121** 4221–36
- [32] Ginsberg N S, Cheng Y-C and Fleming G R 2009 Two-dimensional electronic spectroscopy of molecular aggregates *Acc. Chem. Res.* **42** 1352–63
- [33] Cho M, Scherer N F, Fleming G R and Mukamel S 1992 Photon echoes and four-wave-mixing spectroscopies *J. Chem. Phys.* **96** 5618–29
- [34] Schlau-Cohen G S, Dawlaty J M and Fleming G R 2012 Ultrafast multidimensional spectroscopy: principles and applications to photosynthetic systems *IEEE J. Sel. Top. Quantum Electron.* **18** 283–95
- [35] Borri P, Langbein W, Mørk J and Hvam J M 1999 Heterodyne pump-probe and four-wave mixing in semiconductor optical amplifiers using balanced lock-in detection *Opt. Commun.* **169** 317–24
- [36] Borri P and Langbein W 2007 Four-wave mixing dynamics of excitons in InGaAs self-assembled quantum dots *J. Phys.: Condens. Matter* **19** 295201
- [37] Borri P, Langbein W, Birkedal D, Lyssenko V G and Hvam J M 1997 Nonlinear response of localized excitons: effects of the excitation-induced dephasing *Phys. Status Solidi b* **164** 61–5
- [38] Bergman D J and Stockman M I 2003 Surface plasmon amplification by stimulated emission of radiation: quantum generation of coherent surface plasmons in nanosystems *Phys. Rev. Lett.* **90** 027402
- [39] Kasprzak J, Patton B, Savona V and Langbein W 2011 Coherent coupling between distant excitons revealed by two-dimensional nonlinear hyperspectral imaging *Nature Photon.* **5** 57–63
- [40] Moody G, Siemens M E, Bristow A D, Dai X, Bracker A S, Gammon D and Cundiff S T 2011 Exciton relaxation and coupling dynamics in a GaAs/Al_xGa_{1-x}As quantum well and quantum dot ensemble *Phys. Rev. B* **83** 245316
- [41] Moody G, Siemens M E, Bristow A D, Dai X, Karaiskaj D, Bracker A S, Gammon D and Cundiff S T 2011 Exciton–exciton and exciton–phonon interactions in an interfacial GaAs quantum dot ensemble *Phys. Rev. B* **83** 115324
- [42] Meyer S and Engel V 2000 Non-perturbative wave-packet calculations of time-resolved four-wave-mixing signals *Appl. Phys. B: Lasers Opt.* **71** 293–7
- [43] Yang L and Mukamel S 2008 Two-dimensional correlation spectroscopy of two-exciton resonances in semiconductor quantum wells *Phys. Rev. Lett.* **100** 057402
- [44] Richter M, Ahn K J, Knorr A, Schliwa A, Bimberg D, El-Amine Madjet M and Renger T 2006 Theory of excitation transfer in coupled nanostructures—from quantum dots to light harvesting complexes *Phys. Status Solidi b* **243** 2302–10
- [45] Unold T, Mueller K, Lienau C, Elsaesser T and Wieck A D 2005 Optical control of excitons in a pair of quantum dots coupled by the dipole–dipole interaction *Phys. Rev. Lett.* **94** 137404